# Initial performance of the Radar Echo Telescope for Cosmic Rays: Pathfinder for a next-generation neutrino detector

P. Allison,[1] J. Beatty,[1] D. Besson,[2] A. Connolly,[1] A. Cummings,[3] C. Deaconu,[4] S. De Kockere,[5] K. D. de Vries,[5] D. Frikken,[1] C. Hast,[6] E. Huesca Santiago,[5] C.-Y. Kuo,[7] A. Kyriacou,[2] U. A. Latif,[5] J. Loonen,[5] I. Loudon,[8,9] V. Lukic,[5] C. McLennan,[2] K. Mulrey,[9] J. Nam,[7] K. Nivedita,[9] A. Nozdrina,[2] E. Oberla,[4] S. Prohira,[2,*] J. P. Ralston,[2] M. F. H. Seikh,[2] R. S. Stanley,[5] J. Stoffels,[5] S. Toscano,[8] D. Van den Broeck,[5,10] N. van Eijndhoven,[5] S. Wissel,[3] and R. W. Young[2]

(Radar Echo Telescope)

[1]*Department of Physics, Center for Cosmology and AstroParticle Physics (CCAPP), The Ohio State University, Columbus, Ohio 43210, USA*
[2]*University of Kansas, Lawrence, Kansas 66045, USA*
[3]*Departments of Physics and Astronomy & Astrophysics, Institute for Gravitation and the Cosmos, Pennsylvania State University, University Park, Pennsylvania 16802, USA*
[4]*Enrico Fermi Institute, Kavli Institute for Cosmological Physics, Department of Physics, University of Chicago, Chicago, Illinois 60637, USA*
[5]*Vrije Universiteit Brussel, Dienst ELEM, IIHE, Brussels, Belgium*
[6]*SLAC National Accelerator Laboratory, Menlo Park, California 94025, USA*
[7]*National Taiwan University, Taipei, Taiwan*
[8]*Université Libre de Bruxelles, Brussels, Belgium*
[9]*Department of Astrophysics/IMAPP, Radboud University, P.O. Box 9010, 6500 GL Nijmegen, The Netherlands*
[10]*Vrije Universiteit Brussel, Astrophysical Institute, Brussels, Belgium*

(Received 30 September 2024; accepted 29 June 2026; published 26 October 2026)

The Radar Echo Telescope for Cosmic Rays, a pathfinder instrument for the radar echo method of ultrahigh energy neutrino detection, was initially deployed near Summit Station, Greenland, in May 2023. After a four-week commissioning period, nine days of data were taken before the instrument went offline. In this article, we describe the instrument as it was deployed, and the initial performance of the detector. We show that the technical aspects of running a radar-based particle cascade detector in the ice have been demonstrated. Analysis of the 2023 data informed improvements that were incorporated into the May–August 2024 deployment, which has just concluded at time of writing. Results from the 2024 run will be presented in forthcoming publications.

DOI: 10.1103/c2x7-6gq7

## I. INTRODUCTION

The Radar Echo Telescope for Cosmic Rays (RET-CR) [1] is a pathfinder instrument for the radar echo method of ultrahigh energy (UHE) neutrino detection. When a UHE particle initiates a cascade within a dense material, a short-lived cloud of ionization is created that can reflect incident radio waves. With the radar echo method, a transmitting antenna and receiving antenna(s) are deployed within a large target volume, such as the large ice sheets found in the Arctic and Antarctic, to detect the radar reflections from neutrino initiated cascades. This method will be eventually realized by the Radar Echo Telescope for Neutrinos (RET-N), one of the many current and future instruments planned to probe the neutrino flux with energies above ∼10 PeV [2]. What sets the radar echo method apart from all other current and future technologies is that it is the only *active* method for detecting UHE neutrinos: the signal that is detected is the transmitted signal reflected from the cascade, rather than direct emission (optical, or radio frequency) from the cascade itself. This allows a radar echo detector to lower the energy bound for detection by increasing transmitter output power, and modulation and trigger routines can be employed to more easily separate signal from background.

*Contact author: prohira@ku.edu

*Published by the American Physical Society under the terms of the Creative Commons Attribution 4.0 International license. Further distribution of this work must maintain attribution to the author(s) and the published article's title, journal citation, and DOI. Funded by SCOAP³.*

The radar echo method was first theorized by Blackett and Lovell in 1940 to detect the extensive air showers (EAS) [3] of UHE cosmic ray interactions in the atmosphere with their newly (and secretly) developed radar systems during World War II [4]. These systems had detected anomalous reflections from the upper atmosphere, and the newly theorized EAS seemed a likely explanation. It was demonstrated, however, after years of experimentation and further theoretical work that these reflections were not from UHE cosmic rays, but from meteors in the upper atmosphere, which ionize trails through the thin air at around 100 km altitudes [5–7]. Years later the method was unsuccessfully resurrected to attempt detection of UHE cosmic rays [8–10], at which point it was determined that detection of UHE cosmic rays in the atmosphere with radar was definitively ruled out for a number of reasons. First, the free electron lifetime in air, $\mathcal{O}(10\ \text{ns})$, is too short to persist over the path of an extended cascade, $\mathcal{O}(10\ \text{km})$. Second, collisions between the ionization electrons and air molecules results in a significantly diminished efficiency for the scattered signal [11,12].

However, atmospheric cosmic rays and meteors are not the only objects that produce ionization trails. Neutrinos interacting in dense material produce cascades of secondary particles, which all lose energy to ionization. In a dense material like ice, this ionization is orders of magnitude denser than the ionization produced by cosmic ray interactions in the atmosphere. While low ionization lifetimes and high collisional rates persist in the ice, this increased density means that neutrino-initiated cascades are detectable via radar echo in ice in a way that cosmic rays in the atmosphere are not [13–15] (it should be noted that cosmic-ray detection in air through the primary radio frequency emission from the cascades is well established as presented in the overviews [16,17]; the present article specifically deals with the radar echo method.) This observation has driven the development of RET-N.

Several experiments have been performed to test the method [13,14,18], culminating in experiment T-576 at the SLAC National Accelerator Center, which made the first detection of a particle-induced cascade in a dense material [19,20]. A bunch of $\sim 10^9$ electrons with roughly $10^{10}$ eV per electron was directed into a large plastic target to simulate a $\sim 10^{19}$ eV neutrino in ice. The detection demonstrated that reflections from particle-initiated cascades in a dense material is possible.

RET-CR [1] was developed to test the radar echo method in nature and demonstrate the technology needed to detect neutrino initiated cascades in the same detection material that would house an eventual neutrino detector. RET-CR targets the in-ice component of a UHE cosmic ray EAS. At zenith angles less than ∼30 degrees and energies above ∼10 PeV a significant fraction, >10%, of the primary energy is deposited into the ground within a few cm of the EAS axis [21]. This produces a secondary, dense cascade that mimics a neutrino initiated cascade, but at a far higher event rate than neutrino interactions. Targeting UHE cosmic ray initiated cascades in the ice is therefore a bridge between the successful laboratory detection described above and an eventual neutrino detector, a preliminary description of which was presented in the Snowmass 2021 UHE neutrino summary article [2]. The eventual design of RET-N is beyond the scope of this article, but it will consist of a number of identical radar echo stations in deep ice (as opposed to RET-CR, which is deployed on the surface, owing to the different primary particle being detected) covering a volume of $\mathcal{O}(10\text{–}100\ \text{km}^3)$, on par with other proposed next generation UHE neutrino observatories [2].

RET-CR is a completely novel instrument designed to test a detection technology that has never been attempted in nature before. In this article we detail the initial performance of the instrument as deployed at Summit Station, Greenland in May 2023. We begin by discussing the differences between what was described in our previously published instrument paper [1] and what was actually deployed; primarily a difference in layout geometry and number of stations. We then describe the deployment itself, as well as the commissioning phase data run. We then describe the performance of the various subsystems, and conclude with a discussion of the upgrades and improvements that were realized for the full data run in 2024.

## II. DESCRIPTION OF THE INSTRUMENT

RET-CR can be divided into two main systems: the surface component and the radar component. The surface component consists of autonomous, solar powered stations, each with a pair of scintillator detectors and a dual polarized radio antenna. The radar component consists of a solar power system, a communications system, a central DAQ, a radar transmitter, and radar receivers. The principle of operation of the instrument is unchanged from what was presented in Ref. [1], though some technical aspects are detailed below. The entire instrument was comprised of three surface stations, three downhole receiver strings, and one downhole phased transmitter string, in a layout shown in Fig. 1.

RET-CR operates via triggers from the surface system. A surface station will send a trigger to the radar system when it registers coincident charge deposition in both panels. The window for coincidence is 1 μs. The radar system triggers an event readout when ≥N surface stations trigger within a 1 μs window, with N being set in software. The radar system can also be triggered via software, GPS, or via a selectable edge threshold in the receiver (RX) channels.

### A. Radar system

The radar system is an eight-channel phased transmitter with four receive channels featuring active transmitter

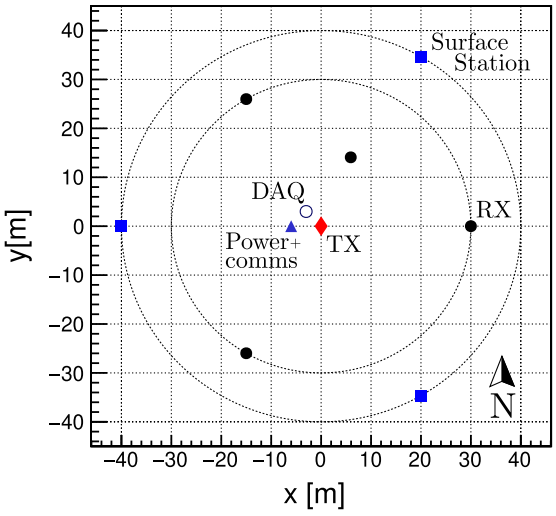



FIG. 1. RET-CR layout as deployed in May 2023. Different system components (surface stations, data acquisition system [DAQ], transmitter [TX], and receiver [RX]) are indicated on the figure, and described in the main text.

cancellation (TC). The heart of the DAQ is a xilinx Radio Frequency Solution On Chip (RFSoC), featuring an eight-channel analog-to-digital converter (ADC) and an eight-channel digital-to-analog converter (DAC). The RFSoC was clocked at ∼3 GHz. A custom-made board breaks out all eight DAC channels and all eight ADC channels. The DAC channels have a software-controlled variable attenuator providing up to 32 dB of attenuation per channel. Four of the DAC channels are used to actively cancel the TX signal in the RX channels by injecting a scaled, time-delayed copy of the transmitted signal into the RX signal path. Overall attenuation of the transmitted signal in the RX of $>80$ dB is achieved. The TX and RX antennas are all identical wide-cylinder dipoles with a 6.35 cm radius. For the eight-channel TX phased array, each antenna is fed by a single 20 W power amplifier, and each pair of power amplifiers is fed by a single channel of the DAC, allowing for pairwise phasing of the transmitted polar angle. The eight TX antennas are separated by ∼0.3 m,[1] deployed such that the midpoint between the fourth and fifth antennas is approximately 10 m deep. Each RX channel consists of an antenna, a combiner for the transmitter cancellation, a ∼60 dB low-noise amplifier, and a bandpass filter from 100–300 MHz. Each RX is lowered down a borehole to a depth of 10 m and a distance of 30 m from the transmitter (TX) borehole. LMR-400 coaxial cable was used for all radio frequency (RF) lines, except for the TX cancellation line, which was LMR-240. The radar system is powered by a triangular solar array with 1.2 kW nominal power per face, and a 200 Ah, 24 V battery buffer. GPS provides accurate timestamping of events, and a Wireless Local Area Network (WLAN) bridge provides telemetry and commanding from Summit Station.

The Field programmable gate array firmware included a software interface for debugging and diagnostic information as well as commanding. The interface allows us to: change the TX frequency and modulation, steer the polar angle of the phased transmitter, send software triggers, run the TX cancellation routine, change the attenuation setting on the DAC channels, enable/disable the RF trigger and set the threshold, select the number of surface stations required to form a trigger, set the delay time between a trigger and an event readout (to ensure enough data has been buffered before readout), and request different levels of debug and diagnostic data. Changing the TX frequency and modulation allows us to observe the reflected signal in different bands. The carrier cancellation finds the optimal amplitude and timing offset to cancel the transmitter in each receive channel simultaneously. A single event record is a header with useful housekeeping information and four records of 32,768 bytes, corresponding to 16,384 samples of data, one per RX channel. Data is readout to a raspberry pi single board computer (SBC) via ethernet for fast transfer and recorded redundantly on two disks before telemetry over WLAN to Summit Station, where it is redundantly recorded once more and transmitted to servers in the U.S. A power distribution system allows for on/off control of the individual power amplifiers via software.

### B. Surface system

A single surface station consists of 2 scintillator panels [22], a cross-pol log periodic dipole antenna [23], a power system consisting of an omnidirectional $4 \times 20$ W solar array with a 10 Ah, 12 V battery buffer, a raspberry pi SBC with redundant storage, and electronics for readout of the scintillators and radio antenna. The SBC controls the readout electronics for the scintillators and radio antenna, the latter of which is repurposed from the CODALEMA experiment [24]. There are three such stations on a 40 m radius from the TX. Communication with the surface stations is achieved via ethernet on a cat-7 cable, with trigger signals sent along a separate cat-7 cable. The scintillator panels were deployed on the surface, and the radio antenna was deployed atop bamboo poles to elevate it approximately 1 m off the surface. Every cosmic ray, RF, and forced/software trigger is sent to every surface station, triggering an event readout of the surface radio.

## III. DEPLOYMENT

The deployment of RET-CR took place in May 2023 with a team of five people. RET-CR is located approximately 6 km north/northeast of Summit Station, Greenland. Summit Station is ideally suited to RET-CR, situated at 3,216 m above sea level at roughly the center of the Greenland Ice

[1]The wavelength of radio changes with depth owing to the changing density and index of refraction of ice, but we ignore these changes over the ∼5 m length of our deployment string.



FIG. 2. RET-CR, as deployed for the 2023 run. Solar panels are evident in the center, and flags denote the buried receivers and transmitter. In the middle distance are smaller solar trees and a surface radio antenna.

Sheet (72.579583, −38.459186). This high elevation, uniform ice facilitates the deposition of a significant fraction of the primary cosmic ray energy into the ice, ideal for maximizing chances of measuring a radar echo.

Station staff assisted in setting up a shelter/work tent at the site. The four boreholes were drilled using a Kovacs Mark-V coring system. The surface stations, including antennas, were assembled and deployed. The radar power system was assembled on site and raised, using guylines set to dead-men anchors to protect from the wind. The WLAN link was established by facing one point of the photovoltaic (PV) triangle directly toward Summit Station and mounting the WLAN antenna at this point. The DAQ, a single Nanuk 975 enclosure with custom bulkhead panels and inlet/outlet vents for thermal regulation, was buried in a $2 \times 2 \times 1$ m snow pit vault covered with plywood, to protect it from blowing snow. A photograph of the deployed instrument is shown in Fig. 2, with the PV array visible at center right, and one of the surface stations in the middle distance. Flags indicate buried elements such as the receiver strings (far right) and cables. The large snow disturbance in the foreground was drifting against our deployment tent, which Summit Station staff had removed at the end of our deployment, just before this photo was taken.

## IV. INITIAL PERFORMANCE

The instrument worked nominally for several hours as soon as it was powered on. By the next day, we noticed that two of the surface stations had powered off. It was concluded that the surface radio electronics were perhaps drawing too much power, and so these were unplugged from the systems for the duration of the deployment. During the commissioning phase one of the surface station trigger lines went offline, though we still had contact with that station via ethernet, and could verify that it was still triggering nominally. Therefore, all of our data was with $N = 2$ surface station logic, though the timestamped triggers for the third station were also recorded and stored. Additionally, only four transmitter channels were powered on at any time, as we noticed very quickly that the DAQ became far hotter than expected with all eight transmitter power amplifiers active.

After a four-week commissioning period, during which the various subsystems were tested and firmware upgrades were written and pushed, a data run commenced. Communication with RET-CR was lost nine days into this data taking run. Subsequent debugging efforts concluded that the system was still powered on, but that the WLAN link was down, and the system was not fully operational, as evidenced by an inability to detect the TX signal from the surface. The DAQ vault was then uncovered to reveal that overheating resulted in the DAQ box melting down approximately one meter into the snow, and severing the WLAN cable, as well as one of the surface station trigger lines, which had become unresponsive some days before. The DAQ itself had reset into a safe mode during the ninth day of the data run and was undamaged.

Our 220 hours of livetime demonstrated several important technical successes. The first and most important of these was the transmitter cancellation. Without active cancellation, the receiver amplifiers would be fully saturated by the direct transmitter signal. To remedy this, a time-delayed and scaled version of the transmitted signal is fed directly into the RX channels before the front-end amplifier to cancel out the incoming TX signal. A firmware/software routine periodically runs to find the optimal cancellation phase and amplitude. The phase and amplitude that are selected are those which optimally cancel out the received transmitter signal. This is the sum total of the direct TX signal, plus all reflected paths from internal reflecting layers, and most prominently, the surface. Therefore, the cancellation phase will vary with environmental factors, such as changes in temperature, or changes

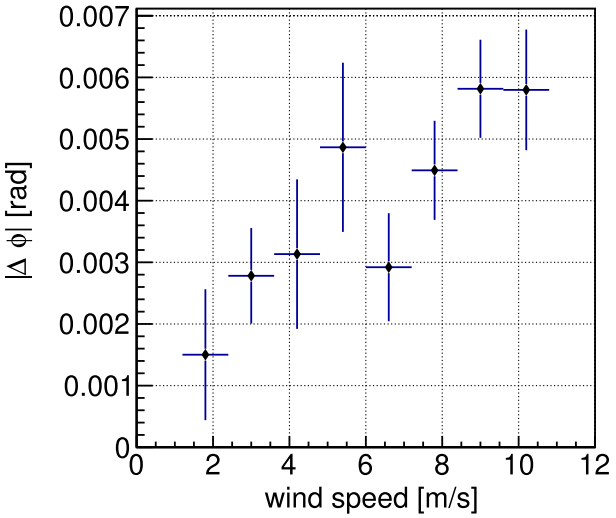



FIG. 3. The magnitude of the change in phase required to cancel the TX signal correlates with wind speed.

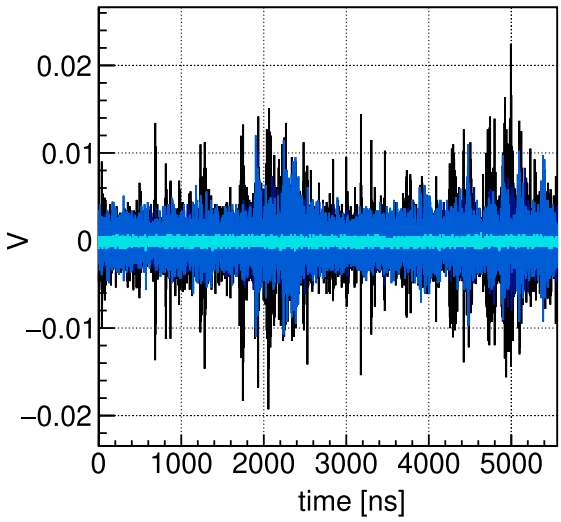



FIG. 4. An example forced trigger event. Data from all four receiver channels are overlaid, the smallest trace being that of an unamplified surface antenna, the other three being the dedicated radar receiver channels. Evident in the data are broadband RF noise spikes from inadequately shielded RF power supplies, which were remedied for the 2024 data run.

of the surface profile through wind or precipitation. Figure 3 shows a qualitative example. Here the magnitude of the change in cancellation phase $|\Delta\phi|$ between hourly runs of the TX cancellation in one receiver is plotted against the local wind speed, as measured at Summit Station.

Even at the relatively modest power of 20 W per channel, the signal received directly by the RX was far higher than the dynamic range input of the front end amplifiers. We were able to use the TC to nearly completely eliminate the TX signal from the RX, even with the TX at full power. The TC happens in two stages. First, the transmitter is set to fractional power, so that the RX amplifiers do not saturate, and the attenuators on the TC DACs are set to a high value. A first stage cancellation is run, to find an approximate value for the cancellation phase and amplitude. Second, the transmitter is increased to full power and the attenuation on the TC DACs are reduced appropriately to best match the amplitude of the incoming signal. Then the second stage TC routine is run, to fully eliminate the signal. We can approximate the cancellation by a simple calculation: a 20 W output, assuming zero gain to the TX and RX, results in a direct TX signal of ∼100 mV at the RX. When the TC is run, the TX is removed to the level of noise, which is nominally ∼10 μV thermal for our band, equating to roughly 80 dB of rejection in power. Figure 6 shows that the cancellation works as expected. In this figure, we plot the unamplified channel with the transmitter on, and we scale this trace by the nominal value, 59 dB, of the receiver amplifiers, to demonstrate the level of the transmitter in the amplified channels (which we cannot show directly, because the amplifiers would saturate). We then compare this level to the transmitter level in the amplified channel, with the TC engaged. These levels are designated by horizontal dashed lines, and their difference for this event, right after the second stage TC was run, is 79.35 dB.

Steering of the beam was demonstrated to work as expected by varying the relative phase of the transmitter antennas and observing the changing amplitude in the receiver strings. Figure 5 shows the arrival time difference between pairs of surface system triggers for a period during commissioning when $N = 3$. The straight-line distance between stations is roughly 70 m, corresponding to a maximum light crossing time of approximately 230 ns. After debugging during commissioning, the data readout

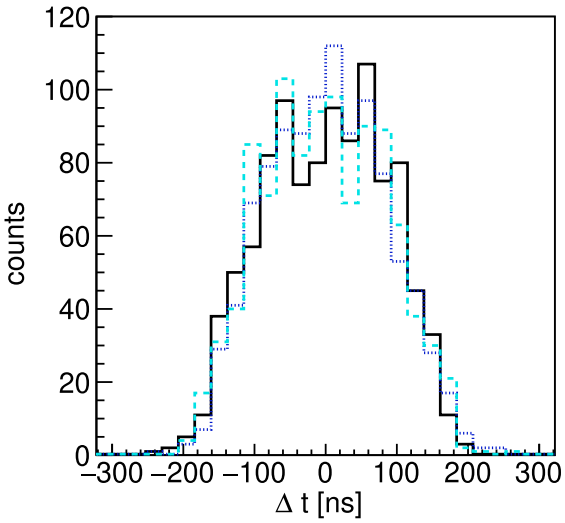



FIG. 5. The time difference in trigger arrival times between pairs of surface systems (each line style/color represents a surface system pair), as recorded on the central radar DAQ. Direct line separation of approximately 70 m sets the maximum light crossing time.

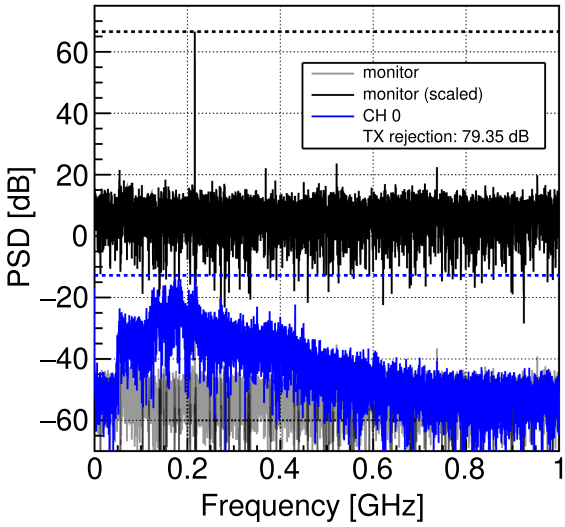



FIG. 6. The transmitter cancellation. Shown is the data from an unamplified monitoring antenna, and this same antenna scaled by the amount of amplification in the amplified reciever channels, to show the transmitter level as it would be in a receiver channel without the cancellation engaged (doing so directly would saturate the receiver amplifier.) Also shown is the data from an amplified channel with the cancellation engaged, giving 79.35 dB of rejection.

was also nominal for the data run, with readout taking ~50 ms per event.

Another issue that became evident during the run was regular broadband radio frequency interference (RFI) that contaminated the data, visible in Fig. 4. We subsequently identified the source of this RFI to be the high current switching power supplies feeding the transmitter amplifiers, which were removed entirely for the subsequent 2024 run.

## V. IMPROVEMENTS FOR 2024

The most critical improvement made after the 2023 run was a redesign of the thermal regulation system. Our design of this initial system was predicated upon a surface deployment, and it allowed us to shed heat sufficiently in such a scenario. However, on arrival at Summit we realized that the filtration system we had designed to keep snow out of the inlet/outlet ports would be insufficient for the local conditions: the inlet filter was ineffective against the finest snow, which could damage/destroy the electronics, and the outlet filter could clog/freeze without regular maintenance. We therefore elected to bury the system, which inhibited cooling, and ultimately caused the system to melt down into the snow. To mitigate this, the 2024 enclosure has an improved, passive thermal regulation system to meet the local conditions. The power amplifiers are bolted to the inside of a large heat sink that forms the lid of the revised electronics enclosure, which was deployed on a platform above the snow surface for 2024.

Other improvements include reconnecting the surface system radio receivers for improved reconstructability of the primary cosmic rays. To achieve this, we doubled the capacity of the surface system power supply. The 2024 system also has two additional surface stations, for a total of 5, with the two additional stations at longer baselines. As deployed in 2023, three RX channels had the full front end chain, with a fourth channel connected, but not buried, and without any front end electronics. The 2024 system included an additional amplified, buried channel, opting to break the symmetry of the layout and deploy one RX at a longer baseline. Finally, the 2024 system has different power regulation to completely remove the main sources of local RFI.

The 2024 data season from May–August has just concluded. The improvements allowed for the system to operate all through the summer, capturing $\mathcal{O}(10^5)$ cosmic ray triggered events. Each event record in the 2024 system contains the data from four amplified channels (three with active carrier cancellation), one unamplified monitoring channel, and five surface stations including the data from surface radio antennas and two scintillator panels per station. Analysis of these data, and details of the improved hardware and firmware, will be presented in forthcoming publications.

## VI. CONCLUSIONS

We have presented the first deployment of RET-CR, and the initial performance of the instrument. RET-CR was deployed for the first time in May 2023, and took nine days of data after a four-week commissioning period. The instrument performed well overall during the data taking period, before going offline, though the data was contaminated by broadband RFI. All problems that were identified during the run were remedied in advance of the data run from May–August 2024, which has recently concluded.

## ACKNOWLEDGMENTS

We sincerely thank the support staff at Summit Station for their tremendous efforts in getting RET-CR into the ice safely and successfully. We also thank K. Hughes and RNO-G Collaboration for their assistance. We thank M. Kauer, C. Wendt, D. Tosi, and IceCube Collaboration for providing our scintillator panels and associated technical support. We thank the CODALEMA experiment for providing our surface radio electronics. We recognize support from The National Science Foundation under Grants No. 2012980, No. 2012989, No. 2306424, No. and 2019597 and the Office of Polar Programs, the Flemish Foundation for Scientific Research FWO-G085820N,

the European Research Council under the European Unions Horizon 2020 research and innovation programme (Grant Agreement No. 805486), the Belgian Funds for Scientific Research (FRS-FNRS), IOP, and the John D. and Catherine T. MacArthur Foundation.

## DATA AVAILABILITY

The data that support the findings of this article are not publicly available. The data are available from the authors upon reasonable request.

[1] S. Prohira *et al.* (Radar Echo Telescope Collaboration), Phys. Rev. D **104**, 102006 (2021).
[2] M. Ackermann *et al.*, J. High Energy Astrophys. **36**, 55 (2022).
[3] P. Auger, Rev. Mod. Phys. **11**, 288 (1939).
[4] P. Blackett and C. Lovell, Proc. R. Soc A **177**, 183 (1941).
[5] A. C. B. Lovell, Notes Rec. R. Soc. London **47**, 119 (1993).
[6] E. V. Appleton, R. Naismith, and I. L. J., Phil. Trans. R. Soc. A **236**, 191 (1937).
[7] E. V. Appleton and J. Piddington, Proc. R. Soc. A **164**, 467 (1938).
[8] P. Gorham, Astropart. Phys. **15**, 177 (2001).
[9] R. Abbasi *et al.*, Nucl. Instrum. Methods Phys. Res., Sect. A **767**, 322 (2014).
[10] R. U. Abbasi *et al.*, Astropart. Phys. **87**, 1 (2017).
[11] M. I. Bakunov, A. V. Maslov, A. L. Novokovskaya, and A. Kryemadhi, Astropart. Phys. **33**, 335 (2010).
[12] J. Stasielak, R. Engel, S. Baur, P. Neunteufel, R. Šmída, F. Werner, and H. Wilczyński, Astropart. Phys. **73**, 14 (2016).
[13] M. Chiba *et al.*, in *15th International Conference on Supersymmetry and the Unification of Fundamental Interactions (SUSY07)* (2007), pp. 850–853, arXiv:0710.4186.
[14] M. Chiba *et al.*, AIP Conf. Proc. **1535**, 45 (2013).
[15] K. D. de Vries, K. Hanson, and T. Meures, Astropart. Phys. **60**, 25 (2015).
[16] F. G. Schröder, Prog. Part. Nucl. Phys. **93**, 1 (2017).
[17] T. Huege and D. Besson, Prog. Theor. Exp. Phys. **2017**, 12A106 (2017).
[18] K. DeVries *et al.*, Proc. Sci. ICRC2017 (**2017**) 1049.
[19] S. Prohira *et al.*, Phys. Rev. D **100**, 072003 (2019).
[20] S. Prohira *et al.*, Phys. Rev. Lett. **124**, 091101 (2020).
[21] S. De Kockere, K. D. de Vries, N. van Eijndhoven, and U. A. Latif, Phys. Rev. D **106**, 043023 (2022).
[22] M. Kauer, T. Huber, D. Tosi, and C. Wendt (IceCube Collaboration), Proc. Sci. ICRC2019 (**2021**) 309. . [arXiv:1908.09860]
[23] D. J. Bacon *et al.* (SKA Collaboration), Pub. Astron. Soc. Aust. **37**, e007 (2020).
[24] B. Revenu, D. Charrier, R. Dallier, A. Escudie, D. García-Fernández, A. Lecacheux, and L. Martin, Proc. Sci. ICRC2017 (**2018**) 416.